Eur. Phys. J. C (2022) 82:197
https://doi.org/10.1140/epjc/s10052-022-10115-4

THE EUROPEAN PHYSICAL JOURNAL C

Regular Article - Experimental Physics I

First design of a crystal-based extraction of 6 GeV electrons for the DESY II Booster Synchrotron

A. Sytov[1,a], G. Kube[2], L. Bandiera[1], P. Cirrone[3], H. Ehrlichmann[2], V. Guidi[1,4], V. Haurylavets[5], M. Romagnoni[1], M. Soldani[1,4], M. Stanitzki[2], M. Tamisari[6], V. Tikhomirov[5], K. Wittenburg[2], A. Mazzolari[1]

[1] INFN Ferrara Division, Via Saragat 1, 44122 Ferrara, Italy
[2] Deutsches Elektronen-Synchrotron DESY, Notkestr. 85, 22607 Hamburg, Germany
[3] INFN Laboratori Nazionali del Sud, Via Santa Sofia 62, 95123 Catania, Italy
[4] Dipartimento di Fisica e Scienze della Terra, Università degli Studi di Ferrara, Via Saragat 1, 44122 Ferrara, Italy
[5] Institute for Nuclear Problems, Belarusian State University, Bobruiskaya 11, 220030 Minsk, Belarus
[6] Dipartimento di Neuroscienze e Riabilitazione, Università degli Studi di Ferrara, Via Luigi Borsari 46, 44121 Ferrara, Italy

Received: 12 November 2021 / Accepted: 8 February 2022 / Published online: 5 March 2022
© The Author(s) 2022

Abstract A proof-of-principle experimental setup for the extraction of 6 GeV electrons from the DESY II Booster Synchrotron using the channeling effect in a bent crystal is elaborated. Various aspects of the experimental setup were investigated in detail, such as the particle beam dynamics during the extraction process, the manufacturing and characterization of bent crystals, and the detection of the extracted beam. In order to optimize the crystal geometry, the overall process of beam extraction was simulated, taking into account the influence of radiation energy losses. As result it is concluded that the multi-turn electron beam extraction efficiency can reach up to 16%. In principle this crystal-based beam extraction technique can be applied at any electron synchrotron in order to provide multi-GeV electron beams in a parasitic mode. This technique will allow to supply fixed-target experiments by intense high-quality monoenergetic electron beams. Furthermore, electron/positron crystal-based extraction from future lepton colliders may provide an access to unique experimental conditions for ultra-high energy fixed-target experiments including searches for new physics beyond the Standard Model.

1 Introduction

Test beam and irradiation facilities are key infrastructures for detector development in High-Energy Physics (HEP). They are dedicated to the qualification of particle detectors, materials, and components prior to their installation in HEP experiments. In Europe there exist three major facilities: the DESY II Test Beam Facility at DESY (Hamburg, Germany) with secondary electron or positron beams between 1 and typically 6 GeV [1] which is based on the DESY II booster synchrotron [2], the DAFNE Beam-Test Facility (BTF) at the Frascati National Laboratory of INFN (LNF) which provides electron or positron beams with tuneable energy from 30 to 800 MeV [3–5] and the PS East and the SPS North Area at CERN which provide primary and secondary hadron and lepton beams between 1 and 400 GeV.

The DESY II synchrotron [6] is used today as the injector for the 3^{rd} generation synchrotron light source PETRA III, ramping up single bunches of about 10^{10} electrons from E_{min} = 0.45 GeV to typically E_{max} = 6.3 GeV, with a possible maximum of 7 GeV. In between two successive fillings which takes typically several minutes in top-up operation, DESY II is used parasitically for test beam operation.

At present these test beams are generated in a double conversion process instead of using a direct extraction of the primary beam. As a first step a bremsstrahlung beam is generated by a 7 μm thick carbon fibre target which is placed in the circulating electron beam of DESY II. As a second step these photons hit a converter target (metal plate), such generating electron/positron pairs which are selected by species and momentum depending on the polarity and the strength of the magnetic field of the subsequent dipole magnet spectrometer. Using such internal target, a low rate of secondary particles can be produced at every bunch crossing, fulfilling the test beam user requirement for a low multiplicity beam. A disadvantage however is the low integrated rate. With three internal targets installed at different locations in the ring, the facility offers three independent beamlines for user operation. Since its inception and start of operation in 1987, the usage of the DESY II Test Beam Facility has continuously

[a] e-mail: sytov@fe.infn.it (corresponding author)

increased. Meanwhile the EU has supported both access and enhancements to the facility within several European grants as e.g. the Horizon 2020-AIDA2020 one [7].

A significant drawback of the present test beam generation mechanism is the finite lifetime of the carbon fibre targets. The experience from wire scanners used in particle beam diagnostics shows that thin wire targets may easily be destroyed. The possible reasons are thermal heating of the wire due to energy loss inside the material, higher order mode heating due to vagrant electromagnetic fields inside the vacuum chambers, sublimation of the target material, and mechanical stress on the wire fork caused e.g. by a movement of the target for alignment purposes [8]. The operational experience with the 7 μm thick wires of the DESY II Test Beam Facility confirms a high risk of target damage which requires a frequent wire replacement of 3–4 wires per station and year. Having in mind the upgrade of the synchrotron light source PETRA III into an ultralow-emittance source PETRA IV being diffraction limited up to X-ray energies of about 10 keV [9] which might imply an upgrade of the existing DESY II injector synchrotron, this will increase the risk of the target wire damage caused by the substantially lower emittance of the new booster ring.

To explore an alternative technique to provide test beams and driven by the interest of the facility users, primary beam extraction schemes are under discussion. A method used at hadron machines is the slow resonant extraction scheme where typically the third-order resonance is intentionally excited by controlling the tune distance and sextupole strength in order to gradually peel off particles from outer to inner regions inside the beam emittance [10,11]. This method is not solely restricted to hadron machines, the scheme has been applied at electron accelerators as e.g. pointed out in Ref. [12].

Another scheme which will be discussed in the following is crystal-assisted beam steering. Since the 1950s, it has been known that the crystalline lattice structure can strongly influence the electromagnetic processes. Such coherent orientational effects in a crystal can be exploited for various applications in accelerator physics as well as for the development of novel X- and gamma-ray crystal-based sources. In the remainder of this article, a design proposal for a proof-of-principle experiment is worked out in order to study a crystal-based beam extraction at the booster synchrotron DESY II. In the future, this scheme could be applied in order to realize a primary beam extraction for the DESY II Test Beam Facility.

2 Crystal-assisted beam steering

The main idea of crystal-assisted beam steering, firstly proposed by Tsyganov in 1976 [13], relies on planar channeling

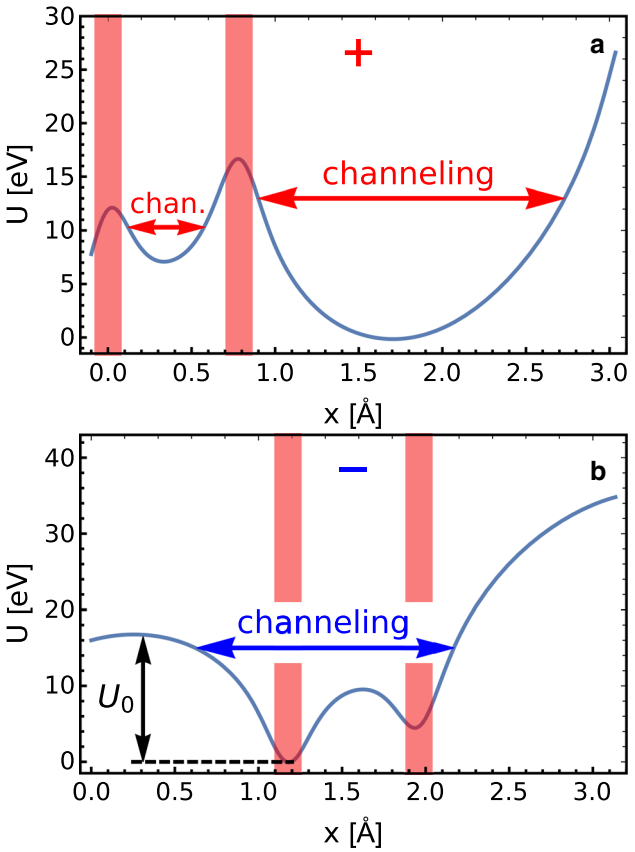

Fig. 1 Channeling region (indicated by horizontal arrows) in the interplanar potential formed by (111) silicon bent crystal planes for particles with charge $+|e|$ (a) and $-|e|$ (b), where e is the charge of the electron. The vertical lines indicate the zone close to the crystal planes at which Coulomb scattering is more intense. Calculations were done for 6 GeV charged particles and a bending radius of 10 cm. U_0 represents the potential well depth

[14]. Planar channeling is a coherent effect of penetration of charged particles in a crystal almost parallel to its planes, when a charged particle is held in a potential well (as shown in Fig. 1) formed by the electric field of two neighboring atomic planes. If a crystal is bent (as illustrated in Fig. 2), the charged beam will be steered since its trajectory is confined under channeling conditions along the bent crystal planes.

Beam steering based on the coherent interaction of charged particle beams with bent crystals has found several applications in accelerator physics. In particular, crystal-based beam collimation and extraction were successfully investigated at several proton synchrotrons, such as the U70, RHIC, Tevatron, SPS and the LHC [15–23]. A new proposal of slow extraction of positrons from DAFNE has been recently published [24]. The main conception of both crystal collimation and extraction consists in interception of beam halo by a bent crystal and consequent deflection under the channeling conditions (as shown in Fig. 3). The difference between collimation and extraction is merely only the device

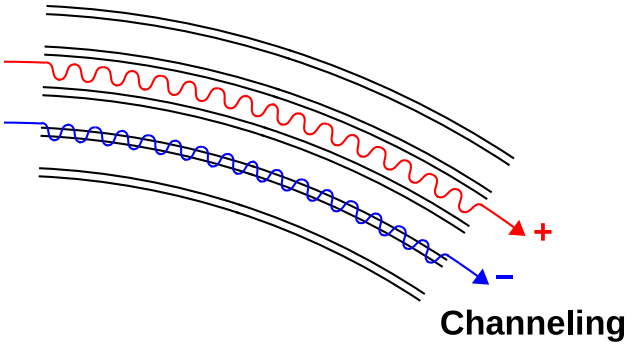

Fig. 2 Schematic illustration of channeling in a bent crystal formed by non-equidistant crystal planes (e.g. (111) planes of a silicon crystal). The signs indicate schematic trajectories either for positively or negatively charged particles

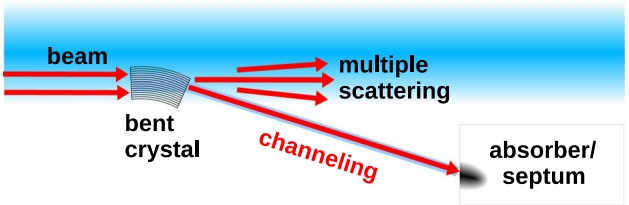

Fig. 3 Schematic illustration of a crystal-based collimation/extraction. The bent crystal deflects the beam onto either an absorber or a septum magnet. A fraction of the beam is not captured under channeling conditions and will be scattered by the bent crystal

onto which the beam halo is deflected, namely absorber and septum magnet, respectively.

The main advantage of such a technique is extraction of the beam in a parasitic mode, i.e. not disturbing the main fraction of the beam, and, therefore, not affecting the main use of the accelerator. Manufacturing and installation of a bent crystal is much cheaper than of any kind of magnetic or electrostatic deflector. Moreover, the extraction efficiency approaches a 100% for positively charged particles. All of this makes a bent crystal an ideal solution for beam extraction for fixed target experiments at modern accelerators.

Though the crystal-based extraction technique is well developed and has been studied for proton beams, it has never been applied for electrons. The main limitation is the significantly lower channeling efficiency for electrons since unlike protons the negatively charged particles move under channeling conditions traversing atomic planes where Coulomb scattering is considerably stronger (compare Fig. 1a and b representing the case of positively and negatively charged particles, respectively). Moreover, unlike proton synchrotrons usually operating at energies from tens of GeV up to few TeV, electron machines usually reach energies of a few GeV, at which the contribution of multiple scattering into the channeling process is much more important because with a decrease in the particle energy, the average value of the angle of multiple incoherent scattering increases. In addition, the radiation losses for electrons may be an important factor, since it may significantly change a particle trajectory in an accelerator leading to beam losses.

However, recent experiments at both the Mainz Microtron MAMI (855 MeV electrons) [25–27] and the SLAC FACET facility (multi-GeV electrons) [28–32] with the new generation of bent crystals [27,33,34] have demonstrated channeling efficiencies in the range from 10 to 40%, i.e. of the same order of magnitude as for protons. Apart from the ultra-low crystal thickness (tens of microns) and very high bending angle (up to few mrad) the crystals possess a very high quality crystalline lattice and uniform bending as well.

In addition to planar channeling, there are other mechanisms for deflecting of both negatively and positively charged particles by a bent crystal, in particular, the Grinenko–Shul'ga mechanism and axial channeling [14,35,36] as well as the effect of multiple volume reflection in one bent crystal [37–40]. These effects may potentially provide high efficiency of the deflection of charged particles of either sign [41–50].

Crystals were developed not only as beam steering devices, but also as innovative X- and γ-ray radiation sources [31,32,49–60], compact electromagnetic calorimeters [55,56,61] and positron sources [62–65] based on the effect of channeling radiation (CR) [66,67]. This type of radiation allows to considerably increase the radiation intensity in comparison with bremsstrahlung. However, the probability of photon emission in such short crystals should not exceed 10–20%, and, therefore, may not significantly affect the extraction efficiency, though must be definitely taken into account. Therefore, such kind of bent crystal should be optimal for the first crystal-based extraction scheme for electrons.

The DESY II booster ring is a well suited synchrotron for the first experimental test of the new technique by the following reasons:

1. The electron beam energy between 450 MeV and 6.3 GeV lies in the energy range already tested in the experiments on channeling mentioned above and is typical for electron synchrotrons existing in the world. Such beams are of interest for testing of nuclear and particle physics detectors and generic detector R&D [1].
2. The upgrade of the Test Beam Facility consisting in the extraction of a primary, and consequently, low-emittance and very intense electron beam into beam test area is an excellent motivation for these studies.
3. The extraction line including septum magnets already exists. Therefore, in general, only a bent crystal has to be installed for the proof-of-principle experiment.

Table 1 DESY II accelerator parameters [6]

Parameter	Value
Ring circumference S_0	292.8 m
Injection energy E_{min}	0.45 GeV
Nominal extraction energy E_0	6 GeV
Number of e^- in the beam N_0	$\sim 10^{10}$
Horizontal emittance ε_x (at 6 GeV)	339 nm rad
Vertical emittance ε_y (at 6 GeV)	35 nm rad
Horizontal tune Q_x	6.7
Vertical tune Q_x	5.7
Energy spread $\sigma_{\delta E/E_0}$	0.977×10^{-3}
Total RF voltage V_s	13.5 MV
Harmonic number h	488
Gamma transition γ_{tr}	6.428

3 The DESY II accelerator and beam extraction scheme

The electron synchrotron DESY II operates mainly as the injector for the 3rd generation synchrotron light source PETRA III. It accelerates and decelerates in a sinusoidal mode with a frequency of 12.5 Hz. The revolution frequency is 1 MHz, the RF frequency 500 MHz, and the bunch length is around 30 ps. The relevant DESY II beam parameters for the beam halo extraction are summarized in Table 1.

The general lattice layout of DESY II has an eight-fold symmetry, each of the eight super periods consists of three FODO cells, and each FODO cell provides a 2220 mm long drift space. From these twenty-four straight sections, eight are equipped with RF-cavities, and the remaining sixteen ones with kicker- and septa magnets for injection and extractions and additional installations as e.g. the vacuum chambers housing the wire targets for the present test beam generation. As mentioned before, for the proof-of-principle experiment an existing extraction region can be utilized which was formerly in use for the DORIS synchrotron which was in operation from 1974 until 2013. The schematic layout of this extraction region is shown in Fig. 4 and will be described in the next paragraph.

3.1 Beam extraction setup

The extraction setup occupies two subsequent straight sections. The first section houses the pulsed deflection device that kicks the beam (or in case of non-pulsed crystal deflection parts of the beam halo) onto a pulsed septum magnet placed downstream. At present it consists of a kicker magnet with a maximum deflection angle of 1.14 mrad in positive x direction if supported by a beam bump, c.f. Fig. 4. The second straight section houses the beam septum which deflects the separated beam portion into the transfer line, i.e. the septum provides space separation between the circulating and extracted beam. The extracted beam passes then through the homogeneous field region of the septum, the circulating one is in the field-free septum region. In order to provide sufficient deflection angle the septum is formed by two individual septum magnets each of 600 mm iron length with a 3 mm thick eddy current shielding, thus separating the region of homogeneous field from the field-free region for the circulating beam. The separated beam portion is then transported along the transfer line, its intensity and beam shape can be measured by beam current monitors and a scintillator based screen monitor.

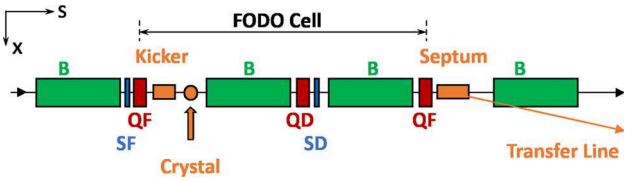

Fig. 4 Scheme of the beam extraction into the former DORIS transfer line. The extraction is embedded in the DESY FODO lattice consisting of dipoles (B) and focusing/defocusing quadrupoles (QF/QD). In addition, the two sextupole families (SF/SD) are indicated. The overall distance from the planned crystal location to the septum position is about 10 m

For the planned experiment the deflecting crystal will be installed in the first straight section. In principle the crystal could be operated as deflection device instead of the kicker magnet. However, in case that the crystal deflection is not sufficient, it can be used in order to support the beam kick towards the septum magnet.

Before designing a dedicated deflection device, in the subsequent paragraph the required deflection angle is estimated based on the lattice parameters at the crystal location and the septum magnet.

3.2 Required deflection

The lattice parameters at the positions of both the deflection device and the septum magnet, which are essential for the estimation of the deflection angle, are summarized in Table 2. With these parameters it is possible to estimate the beam position and the angle at the septum based on the beam parameters at the deflection device, i.e. to study the influence of the crystal on the extracted beam.

Due to the fact that kicker and septum magnets provide only kicks in the horizontal direction, in the subsequent discussion the particle motion will be considered only in this plane. Furthermore, it is assumed that the fraction of the beam to be extracted is the fraction with horizontal coordinates less than -3σ ≈ -6.3 mm of the beam transverse size $\sigma = \sqrt{\varepsilon\beta_x}$. This value would be enough to consider the extraction scheme as non-perturbing, i.e. stripping away

Table 2 Optics parameters at the positions of the deflection device and the septum magnet

Parameter	Deflection device	Septum
Longitudinal position s	148.33 m	158.89 m
Horizontal α-function α_x	1.77	2.17
Vertical α-function α_y	−0.85	−0.43
Horizontal β-function β_x	12.85 m	17.80 m
Vertical β-function β_y	6.07 m	4.22 m
Horizontal phase advance μ_x	3.37	3.63
Vertical phase advance μ_y	2.93	3.11
Horizontal dispersion D_x	1.60 m	1.53 m
Vertical dispersion D_y	0	0
Horizontal dispersion prime D'_x	−0.221	−0.175
Vertical dispersion prime D'_y	0	0

particles with larger horizontal offsets will not affect the operation of DESY II as injector for the synchrotron light source PETRA III during user operation. While the beam orbit is not stable during the DESY II acceleration cycle and moves to the ring inside at higher beam energies, the sign in the -3σ limit indicates that extraction takes place only at higher beam energies for a limited number of turns when the beam has moved far enough towards the inner ring side such that there is a spatial overlap between the beam halo and the extraction crystal.

The horizontal coordinate x and the angle $x' = \theta_x$ are described by both betatron and synchrotron oscillations as:

$$x = x_0 \cos \Psi_x + \delta D_x, \tag{1}$$

$$\theta_x = -\frac{x_0}{\beta_x}(\alpha_x \cos \Psi_x + \sin \Psi_x) + \delta D'_x, \tag{2}$$

where x_0 and Ψ_x are the amplitude and phase of the betatron oscillations, and $\delta = \frac{\Delta p}{p_0}$ is the relative momentum spread with p_0 the design particle momentum and Δp the absolute momentum spread. Assuming Gaussian distributions for the amplitudes of both betatron and synchrotron oscillations, as well as selecting only the coordinates $x < -3\,\sigma$ according to the extraction limit, it is straightforward to generate the distributions of both x and θ_x at the location of the bent crystal as shown in Fig. 5a, b, respectively. The standard deviation of the Gaussian fit of the distribution in Fig. 5b yields a beam angular divergence at the crystal entrance of 0.18 mrad.

The horizontal beam coordinate at the septum can be controlled by the existing extraction kicker (for one dedicated revolution) or the beam bump mentioned beforehand (for a number of revolutions). In order to choose this coordinate one can refer the transverse coordinate distribution at the crystal entrance (see Fig. 5a), which roughly lies between $|3\sigma|$ and $|5\sigma|$. A reasonable choice would be 4σ. Indeed, taking into account the septum boundary thickness being equal to 3 mm (roughly from 4σ to 5σ at the septum magnet position), this will make the entrance into the septum almost unreachable for most of the particles without an angular kick by the deflection device. Therefore, we define the transverse positions of the deflection device and the septum magnet for further consideration to be -3σ and 4σ, respectively. However, it should be underlined that both positions may further be optimized during the experiment.

In order to define the angular kick, one should be able to transport the particles from the location of the deflection device to the location of the septum magnet. In other words, one should be able to transform the distributions in Fig. 5 into the analogical distributions at the septum magnet position using a fixed angular kick. This can be done using the following transport equations [68]:

$$\begin{aligned} x_{sm} &= (x_{cr} - \delta D_{x\,cr})\sqrt{\frac{\beta_{x\,sm}}{\beta_{x\,cr}}}\,(\alpha_{x\,cr}\sin\Delta\Psi_x + \cos\Delta\Psi_x) \\ &\quad + \left(\theta_{x\,cr} - \delta D'_{x\,cr} + \Delta\theta_x\right)\sqrt{\beta_{x\,cr}\beta_{x\,sm}}\sin\Delta\Psi_x \\ &\quad + \delta D_{x\,sm}, \end{aligned} \tag{3}$$

$$\begin{aligned} \theta_{x\,sm} &= -\frac{(1+\alpha_{x\,cr}\alpha_{x\,sm})\sin\Delta\Psi_x + (\alpha_{x\,sm} - \alpha_{x\,cr})\cos\Delta\Psi_x}{\sqrt{\beta_{x\,cr}\beta_{x\,sm}}} \\ &\quad \times (x_{cr} - \delta D_{x\,cr}) + \sqrt{\frac{\beta_{x\,cr}}{\beta_{x\,sm}}}(\cos\Delta\Psi_x - \alpha_{x\,sm}\sin\Delta\Psi_x) \\ &\quad \times \left(\theta_{x\,cr} - \delta D'_{x\,cr} + \Delta\theta_x\right) + \delta D'_{x\,sm}, \end{aligned} \tag{4}$$

where the indices cr and sm indicate the position of deflection device (crystal) and septum magnet, respectively, and $\Delta\Psi_x$ is the betatron phase shift between both locations. x_{cr} and $\theta_{x\,cr}$ are the incident spatial coordinate and angle to the deflection device, respectively. Considering the deflection device having point-like longitudinal extension, one may consider only the change of the angle on the value of the angular kick $\Delta\theta_x$.

By using the distributions from Fig. 5 and Eqs. (3) and (4) one can calculate both the coordinate and angular distribution of the deflected beam at the septum magnet entrance. These distributions with the condition of the angular kick of

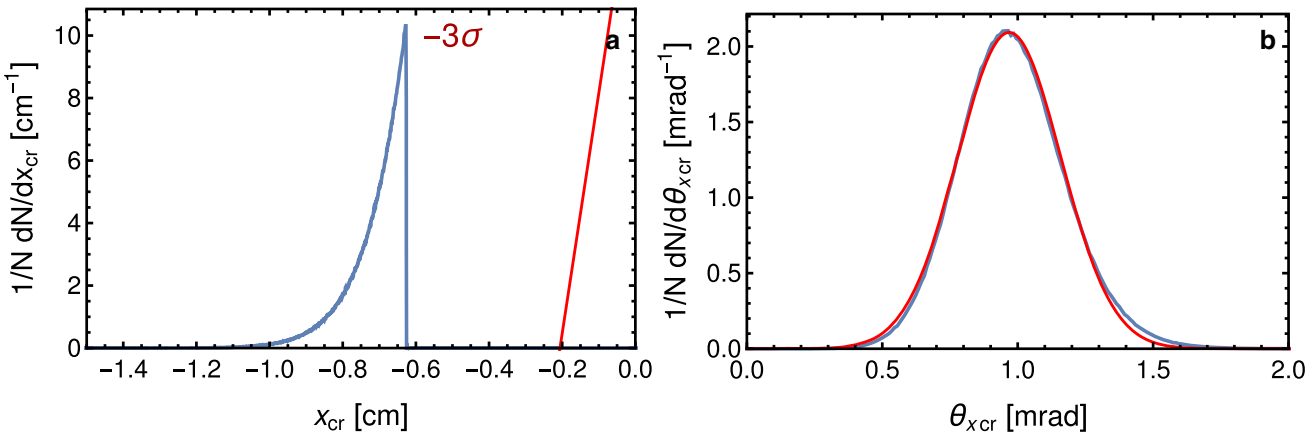

Fig. 5 Transverse **a** spatial coordinate and **b** angular distributions of the beam at the position of the deflection device (bent crystal). The crystal boundary is placed at $x = -3\sigma$. The red curve in **b** indicates the result of a Gaussian fit

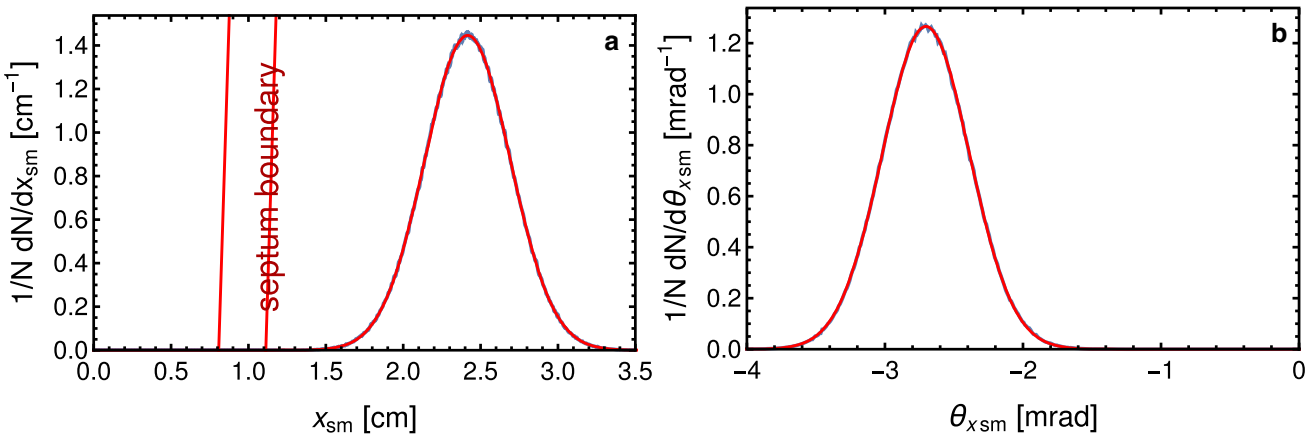

Fig. 6 Transverse **a** spatial coordinate and **b** angular distributions of the beam at the position of the septum magnet with the condition of a constant angular kick of the deflection device of 1.75 mrad. Vertical lines in **a** indicate the septum magnet boundary. The red curves indicate the results of Gaussian fits

1.75 mrad are shown in Fig. 6a-b. The mean values of these distributions are 2.42 cm and −2.7 mrad respectively. The angular kick was chosen to ensure that all the beam being inside 4σ of the coordinate distribution, enters the septum magnet. Some additional gap between the septum magnet boundary and the extracted beam (roughly 1σ thick as shown in Fig. 6a) could be useful for the adjustment of the deflection device and septum magnet positions.

By now we considered an ideal deflection device with a constant angular kick and without energy loss as well. However, if one considers a bent crystal, one should take into account also radiation energy losses, caused by bremsstrahlung or similar effects, since it may cause a considerable trajectory transverse shift. In order to take it into account one should substitute the value δ in Eqs. (3) and (4) by the δ calculated using the energy $E - \Delta E$ instead of its initial value E, where ΔE is the radiation energy loss value. By putting a typical value of radiation energy loss $\Delta E = 100$ MeV covering with some margin both the double height of DESY II RF-bucket and the beam energy increment during a few hundred revolutions in the accelerator, one obtains the following coordinate distribution at the septum magnet entrance shown in Fig. 7 (to be compared with Fig. 6a). One can conclude that the radiation loss may lead to missing the septum magnet by less energetic particles. Since the radiation probability depends on the material thickness, one should make the crystal as short as possible. At the same time, a few MeV of energy loss may not be so important for the extraction process. Moreover, this influence may be reduced by the additional deflection gap mentioned above (Fig. 6a).

4 Simulation code

The CRYSTALRAD simulation code [69–71] is a Monte Carlo code providing fast simulations of both charged particle dynamics and radiation spectra in straight, bent and

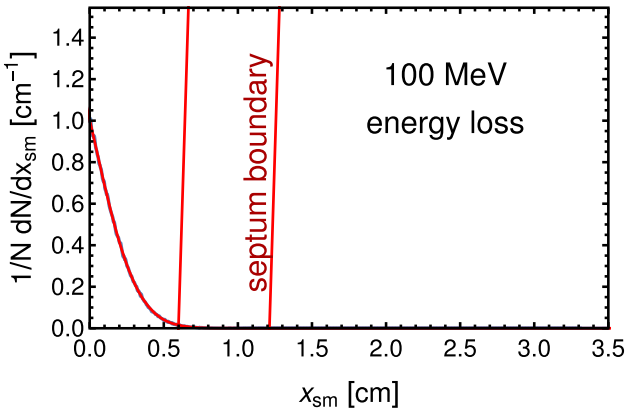

Fig. 7 Transverse coordinate distribution of the beam at the position of the septum magnet with the condition of a constant angular kick of the deflection device of 1.75 mrad, taking into account the energy loss in the deflection device of 100 MeV. The vertical lines indicate the septum magnet boundary. The red curve indicates the result of a Gaussian fit

periodically bent crystal of any material and crystal lattice type with well verified experimentally models of scattering [26,30,74] and radiation [52,69] at the Mainz Mikrotron MAMI for 855 MeV electrons. The code exploits the following approaches.

4.1 A trajectory in a crystal

The charged particle trajectory is calculated assuming a relatively small angle with respect to the crystal planes or atomic strings in the approximation of an averaged atomic potential. It is a quite common approach to simulate channeling effects [14] and has been well validated. A trajectory is calculated by a numerical solution of the trajectory equation using a Runge–Kutta 4th order method [72,73]. Multiple and single Coulomb scattering on a screened (Yukawa) atomic potential as well as single scattering on electrons are randomly simulated at each step of the trajectory equation solution. The Coulomb scattering model includes only the incoherent part of scattering [74,75], while the coherent part is simulated by a trajectory calculation in the averaged atomic potential.

4.2 Radiation losses

The radiation spectrum is calculated using the Baier–Katkov method [76]. This is a widely used model which uses a classical trajectory as an input, but takes into account the quantum recoil of electrons and positrons in the emission of photons. This model allows to calculate the spectra of channeling radiation as well as coherent bremsstrahlung, i.e. the effects caused by the interaction of charged particles with the ordered crystalline structure. The Baier–Katkov method represents itself as a multidimensional numerical integral of the simulated particle trajectory and angles of radiation emission direction depending also on the value of the radiated energy. In CRYSTALRAD we use the Newton–Cotes quadrature rule for the integral of the trajectory as well as the Monte Carlo integration of the radiation emission direction. By calculating this integral for different values of the emitted energy one obtains the radiation spectrum. This spectrum is used for the calculation of the cumulative distribution function, which is consequently applied to randomly generate the event of radiation emission, and, if it occurs, the radiation energy losses. Hereinafter a 1 MeV low-energy cut on radiation production is applied, since a 1 MeV energy loss has almost negligible influence on the accelerator beam dynamics in the case of DESY II.

4.3 Accelerator routine

The accelerator routine [77,78] is needed to simulate the particle dynamics in an accelerator, and, in particular, the crystal-based collimation or extraction scheme. It has been already applied to simulate crystal-based collimation of the SPS (120 GeV), LHC (7 TeV) and FCC-hh (50 TeV) [77,78]. It provides simulations of transverse coordinates and angles at certain longitudinal positions in an accelerator, taking into account both betatron and synchrotron oscillations. This routine exploits the transfer equations (3) and (4) both in the horizontal and in the vertical plane to simulate the accelerator optics as well as the numerical solutions of the differential equations describing the synchrotron motion [68]. A trajectory starts at the crystal entrance surface and finishes at the septum magnet entrance or after the set number of turns in the accelerator is exceeded.

5 Simulations of crystal-based extraction

5.1 Channeling effect simulation

A bent crystal is capable to provide an efficient deflection of the beam halo onto a septum magnet without disturbing the main part of the beam. Electron beam deflection becomes possible due to the channeling effect of electrons in a bent crystal. The efficiency of such deflection strongly depends on the angular divergence of the beam as well as the crystal geometry, i.e. both the crystal thickness and the bending angle.

The physical mechanism of this dependence is the following. The channeling effect is possible only at very low incident angles of particles w.r.t. bent crystal planes, i.e. less than the critical channeling angle (Lindhard angle) [14]:

$$\theta_L = \sqrt{\frac{2U_0}{E}}, \tag{5}$$

where U_0 is the depth of the potential well, shown in Fig. 1b. This angle depends on U_0 becoming lower for higher values of the crystal curvature. The maximal possible value of θ_L at fixed energy is reached for a straight crystal. For the case of a quasi-mosaic Si crystal (111) planes it is equal to 0.088 mrad, which is less but comparable with the angular divergence of the incident beam of 0.18 mrad as calculated above.

The impact of the crystal geometry on the deflection efficiency is determined by two competitive effects. On the one hand it is the effect of dechanneling, i.e. particles escape from the channeling condition, mainly caused by incoherent Coulomb scattering. To minimize this effect, the interaction time between particle and crystal lattice should be kept small, i.e. the crystal should be as short as possible. On the other hand, changing the crystal length at fixed bending angle changes also the radius of curvature of the crystal. Since the bending angle is nearly fixed for our task, increasing the radius reduces the centrifugal force in the frame of reference associated with bent atomic planes and increases the critical channeling angle. Therefore, the crystal thickness has to be increased in order to maximize the channeling acceptance, and consequently, the deflection efficiency. This leads to an optimal crystal thickness value. The existence of optimal parameters for planar channeling of negatively charged particles in a bent crystal has been previously shown in [79,80].

For a preliminary optimization of the thickness a Si (111) bent crystal is chosen since it provides the highest possible efficiency measured experimentally for electrons [26] in the few-GeV energy range. The crystal bending angle has been fixed at the value of θ_b =1.75 mrad as defined above. The incoming beam is the same as in Fig. 5. The simulations of the beam deflection in a bent crystal at different crystal thicknesses has been carried out using the CRYSTALRAD simulation code.

The dependence of the deflection efficiency (an angular kick higher than $\theta_b - \theta_L$ to completely contain the channeling particles) on the crystal thickness is shown in Fig. 8. The maximal efficiency is reached in the range of 120–150 μm thickness. The physical explanation of the channeling effect considered above can be illustrated by the angular distribution of the deflected beam shown in Fig. 9 both in linear and logarithmic scale. One can see that for shortest thicknesses the particle fraction in the dechanneling tale is reduced as well as the number of particles not entered inside the angular acceptance increased, while for the longest ones the picture is inverse. This confirms our physical interpretation described above.

The maximal deflection efficiency is slightly above 1%. Though this number is considerably lower than the efficiency measured previously in the experiments [25–32], it doesn't represents itself as an efficiency of extraction. In fact, not only channeling particles may reach the septum magnet entrance,

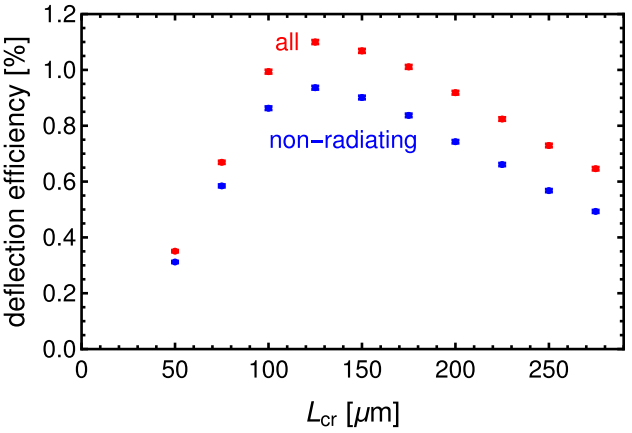

Fig. 8 Deflection efficiency as function of the crystal thickness for a Si crystal bent along the (111) planes with a deflection angle of 1.75 mrad. The lower blue dots represent the fraction of channeled particles that do not emit radiation, while for the upper red points the radiation process is possible. The incoming beam distribution is the same as in Fig. 5

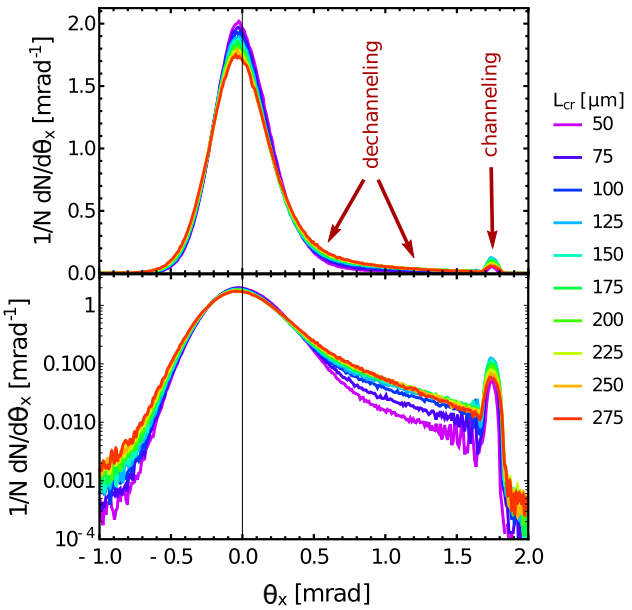

Fig. 9 Angular distribution of the deflected beam as function of the crystal thickness for a Si crystal bent along the (111) planes with a deflection angle of 1.75 mrad in linear (top) and logarithmic (bottom) scale. The incoming beam distribution is the same as in Fig. 5

but also the dechanneled ones. Moreover, the particles that did not enter under the channeling conditions can pass the crystal several times. In other words, the extraction efficiency is a multi-turn efficiency but not a single-turn one. Therefore, in order to calculate and optimize the extraction efficiency one needs to perform complete multi-turn simulations including particle dynamics in an accelerator.

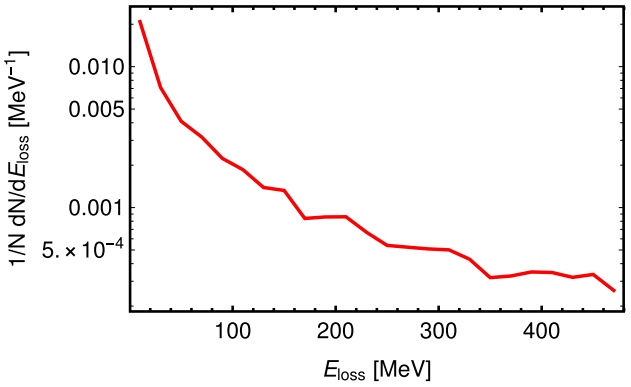

Fig. 10 Radiation energy loss distribution for a 175 μm thick Si crystal, bent along the (111) planes with a deflection angle of 1.75 mrad. The incoming beam distribution is the same as in Fig. 5

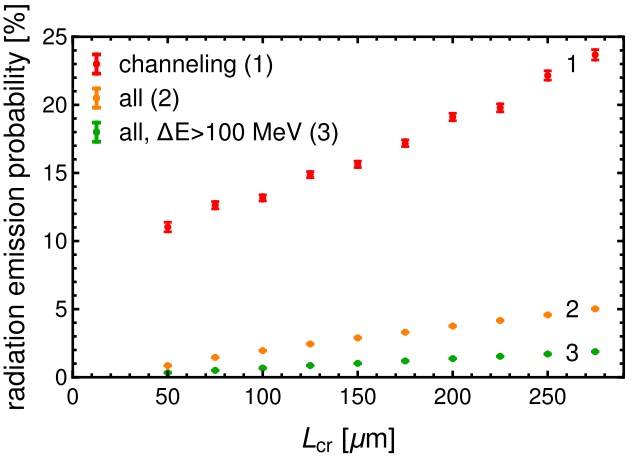

Fig. 11 Radiation emission probability as function of the crystal thickness for (1) the channeled particles which were selected according to $\theta_x > \theta_b - \theta_L$ (red dots), for (2) all particles (yellow dots), and for (3) particles with radiation energy losses exceeding 100 MeV (green dots). The simulations were done for a Si crystal, bent along the (111) planes with a deflection angle of 1.75 mrad. The low-energy cut is 1 MeV. The incoming beam distribution is the same as in Fig. 5

5.2 Radiation energy losses

Radiation energy losses in a bent crystal can considerably modify particle trajectories in an accelerator. Hence it is very important to study both the radiation energy loss distribution and the radiation emission probability for the beam parameters and the crystal geometry considered in this paper.

An example of a radiation energy loss distribution in a 175 μm thick Si bent crystal with θ_b =1.75 mrad is shown in Fig. 10 calculated for the incoming beam from Fig. 5. The form of this distribution is similar to the bremsstrahlung spectrum. Though most of the particles lose few MeV, there is a non-negligible fraction exceeding 100 MeV, which will be directed outside the septum magnet (compare Fig. 7). Therefore, it is important to estimate both the probability of radiation emission for the energies >100 MeV and the total probability, i.e. the entire range of energy losses. These results in dependence of the crystal thickness are shown in Fig. 11.

The total radiation probability (orange in Fig. 11) does not exceed 5%, meaning a rather low fraction of particles though not negligible. The probability of radiation energy losses larger than 100 MeV (green in Fig. 11) is less than 2%. Therefore, most of the particles are not affected by the radiation process and can pass the crystal again if they are not captured under channeling conditions. This makes multi-turn crystal-based extraction of electrons possible.

The total probability of radiation emission by channeling particles selected according to the definition of deflection efficiency (see Fig. 8) is also shown in Fig. 11. As can be seen, channeling radiation gives a considerable rise to the radiation emission probability, even exceeding 20% at higher crystal thicknesses. However, this does not modify strongly the deflection efficiency since the fraction of channeling particles that does not produce radiation is still high as shown in Fig. 9. Moreover, the particles losing low enough energy can be also intercepted by the septum magnet.

Therefore, though the process of radiation emission in a bent crystal needs to be definitely taken into account for crystal-based electron beam extraction, its contribution should not considerably decrease the multi-turn extraction efficiency.

5.3 Multi-turn simulations of crystal-based extraction

The accelerator setup has been simulated with the CRYSTALRAD simulation code using the parameters indicated in Tables 1 and 2, the initial beam distribution at the bent crystal position from Fig. 5, and the crystal parameters from Figs. 8 and 9 for different crystal thickness values. The crystal angular alignment was defined according to the center of the initial angular distribution in Fig. 5b, being 0.97 mrad. The simulated coordinate and angular distribution at the septum magnet entrance after only one passage of the bent crystal are shown in Fig. 12a, b, respectively. The channeling peak position on both distributions coincides with the peak position of an ideally deflected beam from Fig. 5. However, a dechanneling fraction can be also intercepted by a septum magnet. All of these extracted particles need to be included in the extraction efficiency definition.

A considerable part of the particles is randomly scattered by the crystal and is not captured under the channeling conditions as shown in Fig. 13. The multiple scattering angle on the crystal lies in the range of $\sim 50-90$ μrad, i.e. comparable with the critical channeling angle but is considerably lower than the deflection angle required. Consequently, most of randomly scattered particles do not reach the septum magnet entrance, but will be intercepted by its boundary. This

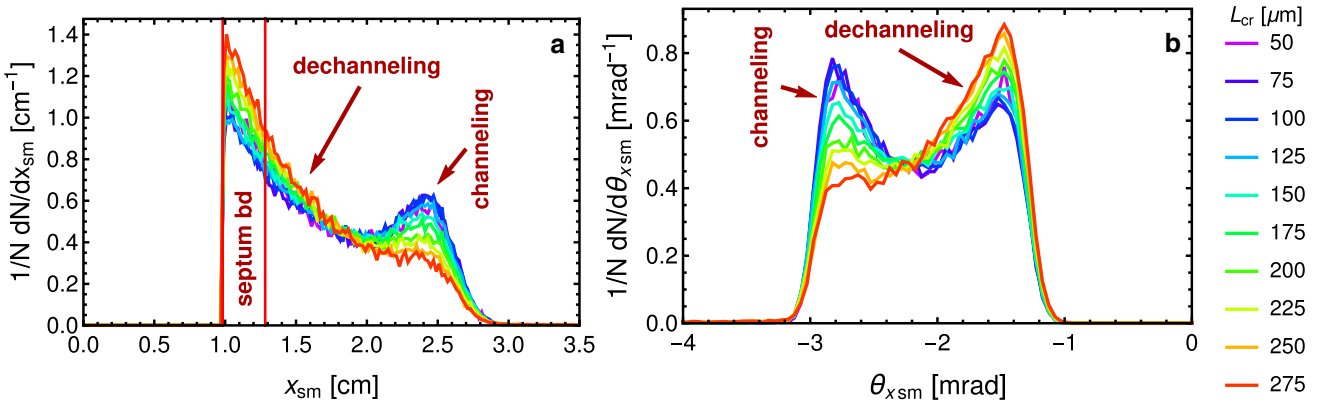

Fig. 12 Transverse **a** coordinate and **b** angular distributions of the beam deflected by a bent crystal at the position of the septum magnet for different crystal thicknesses and Si crystals, bent along the (111) planes with a deflection angle of 1.75 mrad. The vertical lines in (a) indicate the septum magnet boundary. In this figure, only single crystal passage is taken into account

fact confirms that the channeling effect is essential for the crystal-based extraction of an electron beam.

The extraction efficiency is defined as the ratio of the number of extracted particles over the number of particles at the crystal entrance. The number of extracted particles is calculated by using certain cuts applied to certain values at the end of the simulations, namely transverse coordinates, angles, energy, and number of turns in the accelerator. For practical reasons and based on the parameters of the extraction line, the cuts are chosen as described in the following paragraph.

The angular cut is defined to contain the beam in the range of $[-4, 0]$ mrad being in fact the whole extracted beam as shown in Fig. 12b. The maximum number of turns in the accelerator is set to 100, since it is small enough to consider the beam energy as a constant, as well as high enough for charged particles to cross the crystal several times. The energy range follows from the particle energy distribution after 100 revolutions in the accelerator. It is presented in Fig. 14. The energy cut is defined as 6 ± 0.1 GeV. It contains the main part of the beam within the RF-bucket as well as a fraction of particles losing less than 100 MeV. The coordinate cut is simply defined by the coordinates of the septum magnet boundary, as shown in Fig. 13 in the multi-turn coordinate distribution with all the remaining cuts applied. Namely, the coordinates must be $x_{sm} > 1.28$ cm $\approx 5\,\sigma$.

Coordinate and angular distribution at the septum magnet entrance, taking into account the cuts as discussed beforehand, are shown in Fig. 15a, b, respectively. Similarly to the single-passage case (compare Figs. 9, 12), there is an optimal value of the crystal thickness. In order to extract it, one needs to plot the extraction efficiency in dependence of the crystal thickness similarly to the deflection efficiency in Fig. 8. This plot is shown in Fig. 16. Qualitatively, there is a very similar dependence to that in Fig. 8 with the maximal effi-

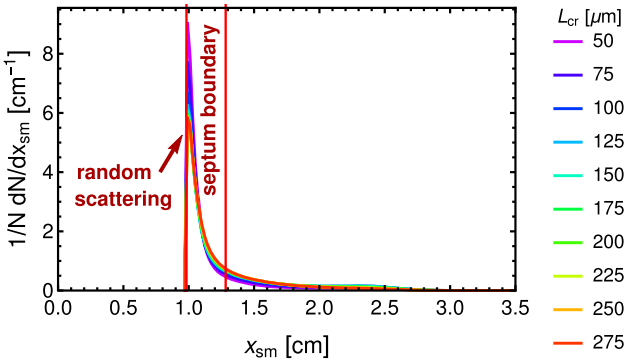

Fig. 13 Multi-turn transverse coordinate distributions of the beam deflected by a bent crystal at the position of the septum magnet for different crystal thicknesses and Si crystals bent along the (111) planes with a deflection angle of 1.75 mrad after 100 revolutions in the accelerator. The vertical lines indicate the septum magnet boundary, both angular and energy cuts are applied

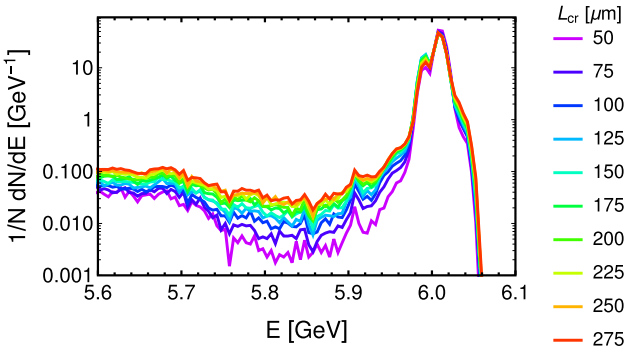

Fig. 14 Energy distributions of the beam, deflected by a bent crystal at the position of the septum magnet for different crystal thicknesses and Si crystals bent along the (111) planes with a deflection angle of 1.75 mrad after 100 revolutions in the accelerator

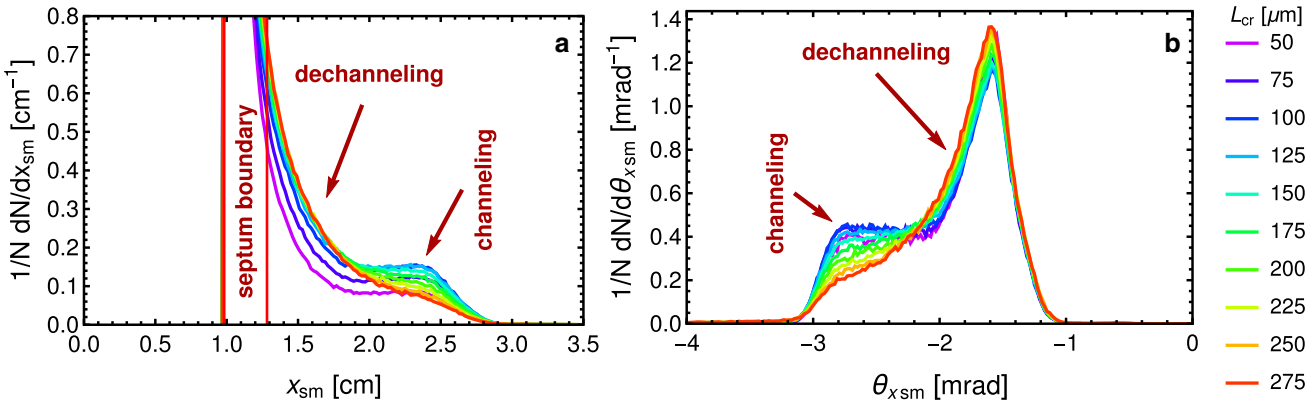

Fig. 15 Multi-turn **a** transverse coordinate and **b** angular distributions of the beam deflected by a bent crystal at the position of the septum magnet for different crystal thicknesses and Si crystals bent along the (111) planes with a deflection angle of 1.75 mrad after 100 revolutions in the accelerator. The vertical lines in **a** indicate the septum magnet boundary, all the cuts are applied

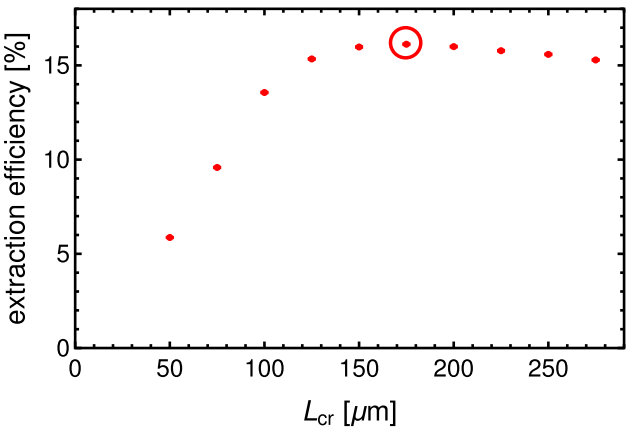

Fig. 16 Extraction efficiency as function of the crystal thickness for Si crystals bent along the (111) planes with a deflection angle of 1.75 mrad. The red circle indicates the optimum case which is described in Table 3

ciency point placed at 175 μm, i.e. being close to the optimal interval estimated above.

The main conclusion for the extraction efficiency in Fig. 16 concerns the maximum value of extraction efficiency that can be experimentally recorded reaching 16.1%. Namely, it is roughly one order of magnitude higher than the single-pass deflection efficiency. This is generally explained by the low multiple scattering angle w.r.t. the angular divergence and the low radiation emission probability as well. It means that if a particle is not captured under the channeling conditions during the first crystal passage, the initial conditions at the next ones may not be significantly different. Therefore, particles can be deflected into the septum magnet under the channeling conditions during the next crystal passages, however keeping in mind that the extraction septum is pulsed and its deflection is optimized for a certain beam energy. Nevertheless the multi-turn crystal-based extraction of electrons is possible and efficient enough.

6 Bent crystal production

6.1 Technologies of bent crystal manufacturing

Bent crystals are fabricated starting from Silicon-On-Insulator bonded wafers [81]. The high purity of these wafers is reached by means of melting-growing methods [82]. The desired shape and thickness from few μm up to few mm can be obtained by depositing of a 100 nm layer of amorphous silicon nitride (Si3N4) onto both faces of the wafer through Low-Pressure Chemical Vapor Deposition followed by photolithography and anisotropic chemical etching of silicon [34].

Once shaped, crystals are mounted on two plugs of a mechanical bender. Bringing both plugs closer together generates a bending moment that makes the crystal bent around the [111] direction. As shown in Fig. 17, due to the so-called quasimosaic effect [83,84], this primary curvature R_p produces a secondary bending of (111) planes R_{qm} which will be used to deflect charge particles. A special technology of a dynamical holder has been developed [26,27] which allows to adjust the crystal curvature after the installation of the crystal into the accelerator vacuum system. This option offers the possibility to optimize the deflection angle during the experiment.

6.2 Bent crystal characterization

A preliminary characterization is done by using high resolution X-ray diffraction, which will allow to reveal an inhomogeneity of the crystal bending and the crystal lattice mosaicity

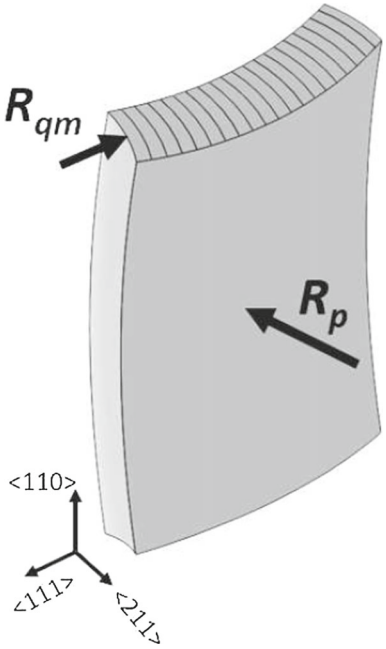

Fig. 17 Thanks to its mechanical anisotropic properties, bending of a silicon crystal along its main size to a radius R_p leads to a secondary bending along its thickness, manifesting with a curvature of radius R_{qm}, which will be used to deflect charge particles by a bent crystal. ⟨111⟩, ⟨110⟩ and ⟨211⟩ represent the directions of crystallographic axes

as well. Both factors in theory can significantly reduce the deflection efficiency. However, the modern technique of crystal manufacturing described before allows to produce bent Si crystals with almost zero mosaicity, without any significant imperfections and with very low inhomogeneity of the crystal curvature, though it hast to be verified for each crystal sample.

A unique way to characterize the crystal is to test it under real conditions, i.e. preferably at similar beam energies with ultra-relativistic electrons. For the planned experiment at DESY II, a suitable test could be performed by using the 855 MeV electron beam of the Mainz Mikrotron MAMI (University of Mainz, Germany). In principle the experimental setup described in Refs. [26,52,74] could be re-used. The low angular divergence of the MAMI beam of 21.4 μrad is advantageous because it is one order of magnitude smaller than the critical channeling angle for sub-GeV energies. For this test experiment and the crystal geometry optimized for DESY II, the simulated angular distribution of the deflected MAMI beam is shown in Fig. 18. As can be seen, the channeling peak which will serve as unique measure for the characterization of the channeling effect in the crystal can clearly be visible.

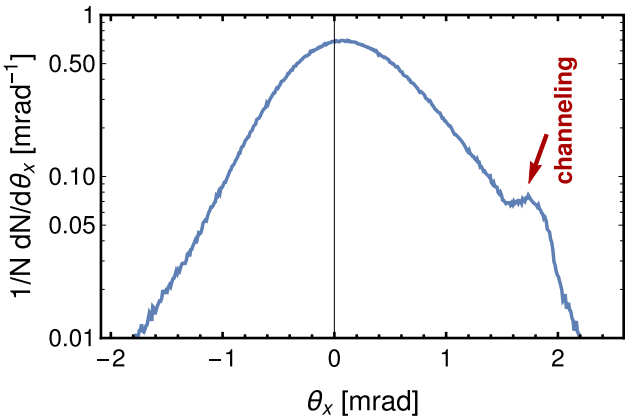

Fig. 18 Angular distribution of a deflected electron beam with an energy of 855 MeV, representing the beam conditions of the Mainz Mikrotron MAMI (University of Mainz, Germany), and a 175 μm thick Si crystal which is bent along the (111) planes with a deflection angle of 1.75 mrad

Table 3 Optimized crystal parameters for the planned experimental setup

Parameter	Value
Bent crystal thickness	175 μm
Bent crystal bending angle	1.75 mrad
Bent crystal transverse position	−0.63 cm
Bent crystal angular alignment	0.97 mrad
Septum magnet transverse position	0.98 cm

7 Preliminary experimental setup design

This section gives a brief overview of the experimental design considerations. The bent crystal will be mounted in an experimental chamber which is embedded in the extraction region into the former DORIS transfer line, c.f. Fig. 4. The optimized crystal parameters for the planned setup are summarized in Table 3. The potential well corresponding to this parameters is shown in Fig. 1b. In order to achieve the required precision for the crystal alignment w.r.t. the beam axis, it will be mounted onto a multi-axis remotely controlled goniometric stage.

The deflected beam will then be injected into the remaining part of the former transfer line which is depicted in Fig. 19. It consists of a bending magnet (MR-08) and a pair of horizontally (QR-02) and vertically (QR12) focusing quadrupoles. Fine alignment of the beam position is possible via steerer magnets in horizontal (SHR10) and vertical (SVR-14 and SVR13) direction. About 35 m away from the extraction point there is a diagnostic station which is installed right behind a shielding wall separating the DESY II accelerator tunnel and the transfer channel. A drawing of this station which was recently commissioned is shown in Fig. 20. In principle, a second diagnostic section could be refurbished

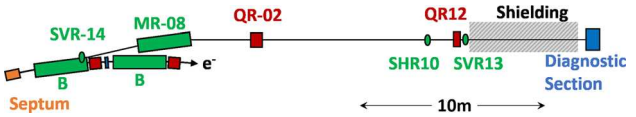

Fig. 19 Overview of the former DORIS transfer line from the extraction region up to the diagnostic section which is located behind a shielding wall in the old transfer tunnel. The line consists of a bending magnet (MR-08) and a pair of horizontally (QR-02) and vertically (QR12) focusing quadrupoles. Fine alignment of the beam position is possible via steerer magnets in horizontal (SHR10) and vertical (SVR-14 and SVR13) direction. The direction of the circulating beam (e^-) is indicated by the arrow. The distance between the extraction point and the detector section is about 35 m

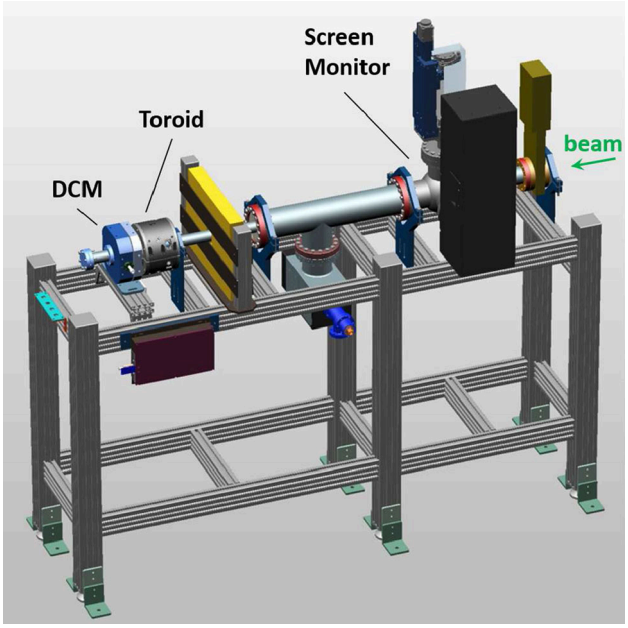

Fig. 20 Diagnostic station for the detection of deflected and extracted beams from the DESY II accelerator. It consists of a screen monitor for the measurement of beam position and shape together with a beam transformer (toroid) and a dark current monitor (DCM) for bunch charge measurements. In this picture, the beam is coming from the right side

which is right in front of the MR-08 dipole. However, at present it is assumed that the station behind the shielding wall will be sufficient for the commissioning of the experiment.

This station includes a scintillating screen monitor for the measurement of the beam position and the shape which is described in Ref. [85]. If the beam hits the scintillator material, light is created in a multistage stochastic process with an intensity distribution which is proportional to the charge density of the incoming beam, resulting in a beam image that can be detected using a conventional area scan camera. In the present monitor setup, $Lu_{2(1-x)}Y_{2x}SiO_5$:Ce (LYSO:Ce) is used as scintillator material, and the intensity profile is detected by means of a standard CMOS camera. Using this type of scintillator it is possible to measure beam profiles for bunch charges down to the level of a few pC. For precise bunch charge measurements, a fast beam transformer (toroid) is used where the beam acts as primary single turn winding in a classical transformer such that it couples inductively to the measurement device. Details about the system which is able to detect bunch charges down to the level 1–2 pC can be found in Refs. [86,87]. For lower charges, the so-called dark current monitor (DCM) will be used. It consists of a resonator made from stainless steel with the frequency of the first monopole mode at 1.3 GHz and a bandwidth of 6.7 MHz, for more details see Refs. [88,89]. Using this kind of device, in principle it is possible to measure bunch charges down to the level of 20 fC.

Using the available beam monitor devices it is possible to optimize the crystal parameters and transfer line settings based on the measured intensity of the deflected beam. In principle it can also be considered to measure the phase space of the extracted beam. To do so, the screen monitor can be used in combination with the two quadrupoles in order to perform a quadrupole scan based emittance measurement, see e.g. Ref. [90]. However, it still has to be investigated if the detection sensitivity, the phase advance of both quadrupoles and the stability of the extracted beam will allow such type of measurements.

8 Conclusions

The first design of a crystal-based extraction of 6 GeV electrons from the DESY II booster synchrotron has been proposed. The main idea of this technique is to extract beam halo from an accelerator in a parasitic mode based on the application of the channeling effect in a bent crystal.

The experimental setup will include a bent crystal which is located in the extraction section of the synchrotron, just behind the extraction kicker and followed by the septum magnet and a transfer line equipped with beam diagnostic monitors as described in the previous section. A bent crystal placed at a horizontal offset of 3σ will deflect beam halo onto the septum magnet. This deflection can be supported by the beam kicker which will shift the beam towards the septum magnet. Both crystal-to-beam and septum-to-beam positions can be adjusted.

The beam distribution at the crystal entrance has been simulated. A crystal bending angle of 1.75 mrad has been chosen to ensure the extraction of charged particles under the channeling conditions.

A multi-turn extraction process has been studied using the CRYSTALRAD simulation code, taking into account radiation processes. It has been shown that though the radiative energy loss may kick out charged particles from an extraction trajectory, the single-turn extraction efficiency will not be affected much and may reach 1% as well. Moreover, since

the average radiation probability does not exceed 5%, multi-turn extraction efficiency is not considerably affected by the radiation process.

The extracted beam distribution has been simulated. The efficiency of beam extraction within ± 0.1 GeV and ± 2 mrad of energy and angular distribution respectively has exceeded 16%.

In general, due to the availability of the beam extraction only for a short moment and at a certain energy while the booster synchrotron is ramping up its energy, the channeling setup at DESY II is considered more as a proof-of-principle experiment for future applications than as an alternative for the existing internal targets. Nevertheless, the future experimental tests of the electron crystal-based extraction technique might raise interest because it can be applied at existing electron synchrotrons worldwide in a straightforward manner. This will make high quality intense electron beams more accessible for a larger community, and consequently, will considerably speed up nuclear and particle physics detectors and generic detector R&D, as well as will be very useful for many projects in high-energy physics requiring fixed-target experiments. Some applications of crystals as X-ray and gamma sources [31,32,49–60], compact electromagnetic calorimeters [55,56,61] and positron sources [62–65] could be also tested in these experiments. Furthermore, since FCC-ee is becoming one of the main after-LHC collider projects, electron/positron crystal-based extraction may provide an access to unique experimental conditions for ultra-high energy fixed-target experiments to measure e.g. CP-violation processes and physics beyond the Standard Model.

Acknowledgements We acknowledge partial support of the INFN through the MC-INFN and the STORM projects. A. Sytov acknowledges support by the European Commission (the TRILLION project within the H2020-MSCA-IF-2020 call, GA. 101032975). M. Romagnoni acknowledges support from the ERC Consolidator Grant SELDOM G.A. 771642. We acknowledge the CINECA award under the ISCRA initiative for the availability of high performance computing resources and support.

Data Availability Statement This manuscript has no associated data or the data will not be deposited. [Authors' comment: All data generated or analysed during this study are included in this published article.]

Open Access This article is licensed under a Creative Commons Attribution 4.0 International License, which permits use, sharing, adaptation, distribution and reproduction in any medium or format, as long as you give appropriate credit to the original author(s) and the source, provide a link to the Creative Commons licence, and indicate if changes were made. The images or other third party material in this article are included in the article's Creative Commons licence, unless indicated otherwise in a credit line to the material. If material is not included in the article's Creative Commons licence and your intended use is not permitted by statutory regulation or exceeds the permitted use, you will need to obtain permission directly from the copyright holder. To view a copy of this licence, visit http://creativecommons.org/licenses/by/4.0/.
Funded by SCOAP[3].

References

1. R. Diener, J. Dreyling-Eschweiler, H. Ehrlichmann, I.M. Gregor, U. Kötz, U. Krämer, N. Meyners, N. Potylitsina-Kube, A. Schütz, P. Schütze, M. Stanitzki, The DESY II test beam facility. Nucl. Instrum. Methods Phys. Res. A **922**, 265 (2019). https://doi.org/10.1016/j.nima.2018.11.133
2. G. Hemmie, DESY II, a new injector for the DESY storage rings PETRA and DORIS II. IEEE Trans. Nucl. Sci. **30**(4), 2028 (1983). https://doi.org/10.1109/TNS.1983.4332706
3. B. Buonomo, G. Mazzitelli, P. Valente, Performance and upgrade of the DAFNE Beam Test Facility (BTF). IEEE Trans. Nucl. Sci. **52**(4), 824 (2005). https://doi.org/10.1109/TNS.2005.852704
4. P. Valente, B. Buonomo, G. Mazzitelli, Diagnostics and upgrade of the DAFNE Beam Test Facility (BTF). Nucl. Phys. Proc. Suppl. **150**, 362 (2006). https://doi.org/10.1016/j.nuclphysbps.2004.06.013
5. B. Buonomo, G. Mazzitelli, F. Murtas, L. Quintieri, P. Valente, A wide range electrons, photons, neutrons beam facility. in *Proceedings of EPAC08, Genoa, Italy, 2008, THPC143*, p. 3321. http://cern.ch/AccelConf/e08/papers/thpc143.pdf
6. https://desy2.desy.de/. Accessed 12 Nov 2021
7. https://aida2020.web.cern.ch/aida2020/. Accessed 12 Nov 2021
8. K. Wittenburg, Beam size measurements using wire scanners. in *Topical Workshop on Emittance Measurements for Light Sources and FELs, 29–30 January 2018, ALBA Synchrotron (Spain)*. https://indico.cells.es/event/128/contributions/133/
9. C.G. Schroer, I. Agapov, W. Brefeld, R. Brinkmann, Y.-C. Chae, H.-C. Chao, M. Eriksson, J. Keil, X. Nuel Gavaldà, R. Röhlsberger, O.H. Seeck, M. Sprung, M. Tischer, R. Wanzenberg, E. Weckert, PETRA IV: the ultralow-emittance source project at DESY. J. Synchrotron Rad. **25**, 1277 (2018). https://doi.org/10.1107/S1600577518008858
10. H.G. Hereward, The possibility of resonant extraction from the CPS. CERN-AR-Int-GS-61-5 (1961). https://cds.cern.ch/record/297121/files/CM-P00064089.pdf. Accessed 12 Nov 2021
11. C.L. Hammer, L.J. Laslett, Resonant beam extraction from an AG synchrotron. Rev. Sci. Instrum. **32**, 144 (1961). https://doi.org/10.1063/1.1717299
12. W. Hillert, The Bonn electron stretcher accelerator ELSA: past and future. Eur. Phys. J. A **28**, 139 (2006). https://doi.org/10.1140/epja/i2006-09-015-4
13. E.N. Tsyganov, Some aspects of the mechanism of a charge particle penetration through a monocrystal. Fermilab TM-682 (1976). https://lss.fnal.gov/archive/test-tm/0000/fermilab-tm-0682.shtml. Accessed 12 Nov 2021
14. J. Lindhard, Influence of crystal lattice on motion of energetic charged particles. Mat. Fys. Medd. Dan. Vid. Selsk. **34**(14), 1–64 (1965). https://gymarkiv.sdu.dk/MFM/kdvs/mfm%2030-39/mfm-34-14.pdf
15. A.G. Afonin, V.T. Baranov, M.K. Bulgakov, Yu.A. Chesnokov, P.N. Chirkov, V.N. Gorlov, I.V. Ivanova, D.M. Krylov, A.N. Lun'kov, V.A. Maisheev, S.F. Reshetnikov, D.A. Savin, E.A. Syshchikov, V.I. Terekhov, I.S. Voinov, I.A. Yazynin, V.B. Ganenko, I.V. Kirillin, N.F. Shul'ga, V.I. Truten', Observation and comparative analysis of proton beam extraction or collimation by different planar channels of a bent crystal. Phys. Rev. ST Accel. Beams **15**, 081001 (2012). https://doi.org/10.1103/PhysRevSTAB.15.081001
16. R.P. Fliller, A. Drees, D. Gassner, L. Hammons, G. McIntyre, S. Peggs, D. Trbojevic, V. Biryukov, Y. Chesnokov, V. Terekhov, RHIC crystal collimation. Nucl. Instrum. Methods Phys. Res. B **234**(1–2), 47 (2005). https://doi.org/10.1016/j.nimb.2005.03.004
17. R.A. Carrigan Jr., D. Chen, G. Jackson, N. Mokhov, C.T. Murphy, S. Baker, A. Bogacz, D. Cline, S. Ramachandran, J. Rhoades, J. Rosenzweig, A. Asseev, V. Biryukov, A. Taratin, J.A. Ellison,

A. Khanzadeev, T. Prokofieva, V. Samsonov, G. Solodov, B. Newberger, E. Tsyganov, H.-J. Shih, W. Gabella, B. Cox, V. Golovatyuk, A. McManus, Beam extraction studies at 900 GeV using a channeling crystal. Phys. Rev. ST Accel. Beams **5**, 043501 (2002). https://doi.org/10.1103/PhysRevSTAB.5.043501

18. N.V. Mokhov, G.E. Annala, A. Apyan, R.A. Carrigan, A.I. Drozhdin, T.R. Johnson, A.M. Legan, R.E. Reilly, V. Shiltsev, D.A. Still, R.J. Tesarek, J. Zagel, S. Peggs, R.W. Assmann, V. Previtali, S. Redaelli, W. Scandale, S. Shiraishi, Y.A. Chesnokov, I.A. Yazynin, V. Guidi, M. Prest, Y.M. Ivanov, Crystal collimation studies at the Tevatron (T-980). Int. J. Mod. Phys. A **25**(Suppl. 1), 98 (2010). https://doi.org/10.1142/S0217751X10049943
19. K. Elsener, G. Fidecaro, M. Gyr, W. Herr, J. Klem, U. Mikkelsen, S.P. Møller, E. Uggerhøj, G. Vuagnin, E. Weisse, Proton extraction from the CERN SPS using bent silicon crystals. Nucl. Instrum. Methods Phys. Res. B **119**(1–2), 215 (1996). https://doi.org/10.1016/0168-583X(96)00239-X
20. W. Scandale, G. Arduini, R. Assmann, C. Bracco, S. Gilardoni, V. Ippolito, E. Laface, R. Losito, A. Masi, E. Metral, V. Previtali, S. Redaelli, M. Silari, L. Tlustos, E. Bagli, S. Baricordi, P. Dalpiaz, V. Guidi, A. Mazzolari, D. Vincenzi, Gianantonio Della Mea, A. Lombardi, D. De Salvador, E. Vallazza, D. Bolognini, S. Hasan, D. Lietti, V. Mascagna, A. Mattera, M. Prest, G. Cavoto, L. Ludovici, D. Mirarchi, R. Santacesaria, P. Valente, F. Murtas, A.G. Afonin, Yu.A. Chesnokov, V.A. Maisheev, I.A. Yazynin, A.D. Kovalenko, A.M. Taratin, A.S. Denisov, Yu.A. Gavrikov, Yu.M. Ivanov, L.P. Lapina, L.G. Malyarenko, V.V. Skorobogatov, V.M. Suvorov, S.A. Vavilov, N. Mokhov, D. Still, G. Robert-Demolaize, T. Markiewicz, M. Oriunno, First results on the SPS beam collimation with bent crystals. Phys. Lett. B **692**(2), 78 (2010). https://doi.org/10.1016/j.physletb.2010.07.023
21. W. Scandale, G. Arduini, R. Assmann, F. Cerutti, S. Gilardoni, E. Laface, R. Losito, A. Masi, E. Metral, D. Mirarchi, S. Montesano, V. Previtali, S. Redaelli, G. Valentino, P. Schoofs, G. Smirnov, E. Bagli, S. Baricordi, P. Dalpiaz, V. Guidi, A. Mazzolari, D. Vincenzi, S. Dabagov, F. Murtas, G. Claps, G. Cavoto, F. Iacoangeli, L. Ludovici, R. Santacesaria, P. Valente, F. Galluccio, A.G. Afonin, M.K. Bulgakov, Yu.A. Chesnokov, V.A. Maisheev, I.A. Yazynin, A.D. Kovalenko, A.M. Taratin, V.V. Uzhinskiy, Yu.A. Gavrikov, Yu.M. Ivanov, L.P. Lapina, V.V. Skorobogatov, W. Ferguson, J. Fulcher, G. Hall, M. Pesaresi, M. Raymond, A. Rose, M. Ryan, G. Robert-Demolaize, T. Markiewicz, M. Oriunno, U. Wienands, Strong reduction of the off-momentum halo in crystal assisted collimation of the SPS beam. Phys. Lett. B **714**, 231 (2012). https://doi.org/10.1016/j.physletb.2012.07.006
22. W. Scandale, G. Arduini, M. Butcher, F. Cerutti, M. Garattini, S. Gilardoni, A. Lechner, R. Losito, A. Masi, D. Mirarchi, S. Montesano, S. Redaelli, R. Rossi, P. Schoofs, G. Smirnov, G. Valentino, D. Breton, L. Burmistrov, V. Chaumat, S. Dubos, J. Maalmi, V. Puill, A. Stocchi, E. Bagli, L. Bandiera, G. Germogli, V. Guidi, A. Mazzolari, S. Dabagov, F. Murtas, F. Addesa, G. Cavoto, F. Iacoangeli, L. Ludovici, R. Santacesaria, P. Valente, F. Galluccio, A.G. Afonin, Yu.A. Chesnokov, A.A. Durum, V.A. Maisheev, Yu.E. Sandomirskiy, A.A. Yanovich, A.D. Kovalenko, A.M. Taratin, A.S. Denisov, Yu.A. Gavrikov, Yu.M. Ivanov, L.P. Lapina, L.G. Malyarenko, V.V. Skorobogatov, T. James, G. Hall, M. Pesaresi, M. Raymond, Observation of channeling for 6500 GeV/c protons in the crystal assisted collimation setup for LHC. Phys. Lett. B **758**, 129 (2016). https://doi.org/10.1016/j.physletb.2016.05.004
23. S. Redaelli, M. Butcher, C. Barreto, R. Losito, A. Masi, D. Mirarchi, S. Montesano, R. Rossi, W. Scandale, P. Serrano Galvez, G. Valentino, F. Galluccio, First observation of ion beam channeling in bent crystals at multi-TeV energies. Eur. Phys. J. C **81**, 142 (2021). https://doi.org/10.1140/epjc/s10052-021-08927-x
24. M. Garattini, D. Annucci, O.R. Blanco-Garcia, P. Gianotti, S. Guiducci, A. Liedl, M. Raggi, P. Valente, Crystal slow extraction of positrons from DAΦNE: the SHERPA project (2021). arXiv:2110.02816v1
25. A. Mazzolari, E. Bagli, L. Bandiera, V. Guidi, H. Backe, W. Lauth, V. Tikhomirov, A. Berra, D. Lietti, M. Prest, E. Vallazza, D. De Salvador, Steering of a sub-GeV electron beam through planar channeling enhanced by rechanneling. Phys. Rev. Lett. **112**, 135503 (2014). https://doi.org/10.1103/PhysRevLett.112.135503
26. A.I. Sytov, L. Bandiera, D. De Salvador, A. Mazzolari, E. Bagli, A. Berra, S. Carturan, C. Durighello, G. Germogli, V. Guidi, P. Klag, W. Lauth, G. Maggioni, M. Prest, M. Romagnoni, V.V. Tikhomirov, E. Vallazza, Steering of sub-GeV electrons by ultrashort Si and Ge bent crystals. Eur. Phys. J. C **77**, 901 (2017). https://doi.org/10.1140/epjc/s10052-017-5456-7
27. D. De Salvador, S. Carturan, A. Mazzolari, E. Bagli, L. Bandiera, C. Durighello, G. Germogli, V. Guidi, P. Klag, W. Lauth, G. Maggioni, M. Romagnoni, A. Sytov, Innovative remotely-controlled bending device for thin silicon and germanium crystals. J. Instrum. **13**(04), C04006 (2018). https://doi.org/10.1088/1748-0221/13/04/C04006
28. U. Wienands, T.W. Markiewicz, J. Nelson, R.J. Noble, J.L. Turner, U.I. Uggerhøj, T.N. Wistisen, E. Bagli, L. Bandiera, G. Germogli, V. Guidi, A. Mazzolari, R. Holtzapple, M. Miller, Observation of deflection of a beam of multi-GeV electrons by a thin crystal. Phys. Rev. Lett. **114**, 074801 (2015). https://doi.org/10.1103/PhysRevLett.114.074801
29. T.N. Wistisen, U.I. Uggerhøj, U. Wienands, T.W. Markiewicz, R.J. Noble, B.C. Benson, T. Smith, E. Bagli, L. Bandiera, G. Germogli, V. Guidi, A. Mazzolari, R. Holtzapple, S. Tucker, Channeling, volume reflection, and volume capture study of electrons in a bent silicon crystal. Phys. Rev. Accel. Beams **19**, 071001 (2016). https://doi.org/10.1103/PhysRevAccelBeams.19.071001
30. T.N. Wistisen, R.E. Mikkelsen, U.I. Uggerhøj, U. Wienands, T.W. Markiewicz, S. Gessner, M.J. Hogan, R.J. Noble, R. Holtzapple, S. Tucker, V. Guidi, A. Mazzolari, E. Bagli, L. Bandiera, A. Sytov, Observation of quasichanneling oscillations. Phys. Rev. Lett. **119**, 024801 (2017). https://doi.org/10.1103/PhysRevLett.119.024801
31. U. Wienands, S. Gessner, M.J. Hogan, T.W. Markiewicz, T. Smith, J. Sheppard, U.I. Uggerhøj, J.L. Hansen, T.N. Wistisen, E. Bagli, L. Bandiera, G. Germogli, A. Mazzolari, V. Guidi, A. Sytov, R.L. Holtzapple, K. McArdle, S. Tucker, B. Benson, Channeling and radiation experiments at SLAC. Nucl. Instrum. Methods Phys. Res. B **402**, 11 (2017). https://doi.org/10.1016/j.nimb.2017.03.097
32. U. Wienands, S. Gessner, M. J. Hogan, T. Markiewicz, T. Smith, J. Sheppard, U.I. Uggerhøj, C.F. Nielsen, T. Wistisen, E. Bagli, L. Bandiera, G. Germogli, A. Mazzolari, V. Guidi, A. Sytov, R.L. Holtzapple, K. McArdle, S. Tucker, B. Benson, The SLAC T513-E212-T523 Collaboration, Channeling and radiation experiments at SLAC. Int. J. Mod. Phys. A **34**(34), 1943006 (2019). https://doi.org/10.1142/S0217751X19430061
33. V. Guidi, A. Mazzolari, D. De Salvador, A. Carnera, Silicon crystal for channelling of negatively charged particles. J. Phys. D Appl. Phys. **42**(18), 182005 (2009). https://doi.org/10.1088/0022-3727/42/18/182005
34. G. Germogli, A. Mazzolari, L. Bandiera, E. Bagli, V. Guidi, Manufacturing and characterization of bent silicon crystals for studies of coherent interactions with negatively charged particles beams. Nucl. Instrum. Methods Phys. Res. B **355**, 81 (2015). https://doi.org/10.1016/j.nimb.2015.03.017
35. A.A. Grinenko, N.F. Shul'ga, Turning a beam of high-energy charged particles by means of scattering by atomic rows of a curved crystal. J. Exp. Theor. Phys. Lett. **54**, 524 (1991). http://jetpletters.ru/ps/1265/article_19143.shtml. Accessed 12 Nov 2021
36. N.F. Shul'ga, A.A. Greenenko, Multiple scattering of ultrahigh-energy charged particles on atomic strings of a bent crystal. Phys. Lett. B **353**, 373 (1995). https://doi.org/10.1016/0370-2693(95)00496-8

37. V. Tikhomirov, Multiple volume reflection from different planes inside one bent crystal. Phys. Lett. B **655**, 217 (2007)
38. V.V. Tikhomirov, Amplification of volume reflection by crystal axes. Probl. Atom. Sci. Technol. **N3**(1), 164 (2007). http://dspace.nbuv.gov.ua/handle/123456789/110932. Accessed 12 Nov 2021
39. V.V. Tikhomirov, A.I. Sytov, Multiple volume reflection in one crystal as an origin of significant scattering intensity and radiation power increase. Nucl. Instrum. Methods Phys. Res. B **309**, 109 (2013). https://doi.org/10.1016/j.nimb.2013.01.068
40. A.I. Sytov, V.V. Tikhomirov, A.S. Lobko, Crystal collimator systems for high energy frontier. Phys. Rev. Accel. Beams **20**, 071001 (2017). https://doi.org/10.1103/PhysRevAccelBeams.20.071001
41. W. Scandale, A. Vomiero, S. Baricordi, P. Dalpiaz, M. Fiorini, V. Guidi, A. Mazzolari, G. Della Mea, R. Milan, G. Ambrosi, B. Bertucci, W.J. Burger, P. Zuccon, G. Cavoto, C. Luci, R. Santacesaria, P. Valente, E. Vallazza, A.G. Afonin, Y.A. Chesnokov, V.A. Maisheev, I.A. Yazynin, A.D. Kovalenko, A.M. Taratin, A.S. Denisov, Y.A. Gavrikov, Y.M. Ivanov, L.P. Lapina, L.G. Malyarenko, V.V. Skorobogatov, V.M. Suvorov, S.A. Vavilov, D. Bolognini, S. Hasan, A. Mozzanica, M. Prest, High-efficiency deflection of high-energy protons through axial channeling in a bent crystal. Phys. Rev. Lett. **101**, 164801 (2008). https://doi.org/10.1103/PhysRevLett.101.164801
42. W. Scandale, A. Vomiero, E. Bagli, S. Baricordi, P. Dalpiaz, M. Fiorini, V. Guidi, A. Mazzolari, D. Vincenzi, R. Milan, Gianantonio Della Mea, E. Vallazza, A.G. Afonin, Yu.A. Chesnokov, V.A. Maisheev, I.A. Yazynin, V.M. Golovatyuk, A.D. Kovalenko, A.M. Taratin, A.S. Denisov, Yu.A. Gavrikov, Yu.M. Ivanov, L.P. Lapina, L.G. Malyarenko, V.V. Skorobogatov, V.M. Suvorov, S.A. Vavilov, D. Bolognini, S. Hasan, A. Mattera, M. Prest, S. Shiraishi, High-efficiency deflection of high-energy negative particles through axial channeling in a bent crystal. Phys. Lett. B **680**, 301 (2009). https://doi.org/10.1016/j.physletb.2009.09.009
43. L. Bandiera, A. Mazzolari, E. Bagli, G. Germogli, V. Guidi, A. Sytov, I.V. Kirillin, N.F. Shul'ga, A. Berra, D. Lietti, M. Prest, D. De Salvador, E. Vallazza, Relaxation of axially confined 400 GeV/c protons to planar channeling in a bent crystal. Eur. Phys. J. C **76**, 80 (2016). http://dx.doi.org/10.1140/epjc/s10052-016-3899-x
44. L. Bandiera, I.V. Kyryllin, C. Brizzolari, R. Camattari, N. Charitonidis, D. De Salvador, V. Guidi, V. Mascagna, A. Mazzolari, M. Prest, M. Romagnoni, N.F. Shul'ga, M. Soldani, A. Sytov, E. Vallazza, Investigation on steering of ultrarelativistic $e^{\pm}$ beam through an axially oriented bent crystal. Eur. Phys. J. C **81**, 238 (2021). https://doi.org/10.1140/epjc/s10052-021-09021-y
45. W. Scandale, A. Vomiero, E. Bagli, S. Baricordi, P. Dalpiaz, M. Fiorini, V. Guidi, A. Mazzolari, D. Vincenzi, R. Milan, G. Della Mea, E. Vallazza, A.G. Afonin, Yu.A. Chesnokov, V.A. Maisheev, I.A. Yazynin, V.M. Golovatyuk, A.D. Kovalenko, A.M. Taratin, A.S. Denisov, Yu.A. Gavrikov, Yu.M. Ivanov, L.P. Lapina, L.G. Malyarenko, V.V. Skorobogatov, V.M. Suvorov, S.A. Vavilov, D. Bolognini, S. Hasan, A. Mattera, M. Prest, V.V. Tikhomirov, First observation of multiple volume reflection by different planes in one bent silicon crystal for high-energy protons. Phys. Lett. B **682**(3), 274 (2009). https://doi.org/10.1016/j.physletb.2009.11.026
46. V. Guidi, A. Mazzolari, V. Tikhomirov, On the observation of multiple volume reflection from different planes inside one bent crystal. J. Appl. Phys. **107**, 114908 (2010). https://doi.org/10.1063/1.3407526
47. W. Scandale, A. Vomiero, E. Bagli, S. Baricordi, P. Dalpiaz, M. Fiorini, V. Guidi, A. Mazzolari, D. Vincenzi, R. Milan, G. Della Mea, E. Vallazza, A.G. Afonin, Yu.A. Chesnokov, V.A. Maisheev, I.A. Yazynin, A.D. Kovalenko, A.M. Taratin, A.S. Denisov, Yu.A. Gavrikov, Yu.M. Ivanov, L.P. Lapina, L.G. Malyarenko, V.V. Skorobogatov, V.M. Suvorov, S.A. Vavilov, D. Bolognini, S. Hasan, A. Mattera, M. Prest, V.V. Tikhomirov, Observation of multiple volume reflection by different planes in one bent silicon crystal for high-energy negative particles. Europhys. Lett. **93**(5), 56002 (2011). https://doi.org/10.1209/0295-5075/93/56002
48. A.G. Afonin, V.T. Baranov, M.K. Bulgakov, I.S. Voinov, V.N. Gorlov, I.V. Ivanova, D.M. Krylov, A.N. Lun'kov, V.A. Maisheev, S.F. Reshetnikov, D.A. Savin, E.A. Syshchikov, V.I. Terekhov, Yu.A. Chesnokov, P.N. Chirkov, I.A. Yazynin, Collimation of the circulating beam in the U-70 synchrotron by means of the reflection of particles in crystals with axial orientation. JETP Lett. **93**, 187 (2011). https://doi.org/10.1134/S0021364011040023
49. V. Guidi, L. Bandiera, V. Tikhomirov, Radiation generated by single and multiple volume reflection of ultrarelativistic electrons and positrons in bent crystals. Phys. Rev. A **86**, 042903 (2012). https://doi.org/10.1103/PhysRevA.86.042903
50. L. Bandiera, E. Bagli, V. Guidi, A. Mazzolari, A. Berra, D. Lietti, M. Prest, E. Vallazza, D. De Salvador, V. Tikhomirov, Broad and intense radiation accompanying multiple volume reflection of ultrarelativistic electrons in a bent crystal. Phys. Rev. Lett. **111**, 255502 (2013). https://doi.org/10.1103/PhysRevLett.111.255502
51. L. Bandiera, E. Bagli, G. Germogli, V. Guidi, A. Mazzolari, H. Backe, W. Lauth, A. Berra, D. Lietti, M. Prest, D. De Salvador, E. Vallazza, V. Tikhomirov, Investigation of the electromagnetic radiation emitted by sub-GeV electrons in a bent crystal. Phys. Rev. Lett. **115**, 025504 (2015). https://doi.org/10.1103/PhysRevLett.115.025504
52. L. Bandiera, A. Sytov, D. De Salvador, A. Mazzolari, E. Bagli, R. Camattari, S. Carturan, C. Durighello, G. Germogli, V. Guidi, P. Klag, W. Lauth, G. Maggioni, V. Mascagna, M. Prest, M. Romagnoni, M. Soldani, V.V. Tikhomirov, E. Vallazza, Investigation on radiation generated by sub-GeV electrons in ultrashort silicon and germanium bent crystals. Eur. Phys. J. C **81**, 284 (2021). https://doi.org/10.1140/epjc/s10052-021-09071-2
53. L. Bandiera, E. Bagli, A. Berra, D. Bolognini, P. Dalpiaz, G. Della Mea, D. De Salvador, V. Guidi, S. Hasan, D. Lietti, A. Mazzolari, M. Prest, V. Tikhomirov, E. Vallazza, On the radiation accompanying volume reflection. Nucl. Instrm. Methods in Phys. Res. B **309**, 135 (2013). https://doi.org/10.1016/j.nimb.2013.02.029
54. L. Bandiera, E. Bagli, G. Germogli, V. Guidi, A. Mazzolari, H. Backe, W. Lauth, A. Berra, D. Lietti, M. Prest, D. De Salvador, E. Vallazza, V. Tikhomirov, PoS **(ICHEP2016)**, 069 (2016). https://pos.sissa.it/282/069/pdf
55. L. Bandiera, V.V. Tikhomirov, M. Romagnoni, N. Argiolas, E. Bagli, G. Ballerini, A. Berra, C. Brizzolari, R. Camattari, D. De Salvador, V. Haurylavets, V. Mascagna, A. Mazzolari, M. Prest, M. Soldani, A. Sytov, E. Vallazza, Phys. Rev. Lett. **121**, 021603 (2018). https://doi.org/10.1103/PhysRevLett.121.021603
56. L. Bandiera, V. Haurylavets, V. Tikhomirov, Compact electromagnetic calorimeters based on oriented scintillator crystals. Nucl. Instrum. Methods Phys. Res. A **936**, 124 (2019). https://doi.org/10.1016/j.nima.2018.07.085
57. V.G. Baryshevsky, I.Ya. Dubovskaya, A.O. Grubich, Generation of γ-quanta by channeled particles in the presence of a variable external field. Phys. Lett. A **77**(1), 61 (1980). https://doi.org/10.1016/0375-9601(80)90637-4
58. V.V. Kaplin, S.V. Plotnikov, S.A. Vorobijev, Radiation of channeled particles in deformed crystals. Zh. Tech. Fiz. **50**, 1079 (1980) [Sov. Phys. Tech. Phys. **25**, 650 (1980)]
59. M. Tabrizi, A.V. Korol, A.V. Solov'yov, W. Greiner, Feasibility of an electron-based crystalline undulator. Phys. Rev. Lett. **98**, 164801 (2007). https://doi.org/10.1103/PhysRevLett.98.164801
60. R. Camattari, L. Bandiera, V. Tikhomirov, M. Romagnoni, E. Bagli, G. Germogli, A. Sytov, T. Maiolino, M. Tamisari, A. Mazzolari, V. Guidi, G. Cavoto, Silicon crystalline undulator prototypes: manufacturing and x-ray characterization. Phys. Rev. Accel. Beams **22**, 044701 (2019). https://doi.org/10.1103/PhysRevAccelBeams.22.044701

61. M. Moulson for the KLEVER Project, KLEVER: an experiment to measure BR($K_L \to \pi^0 \nu\bar{\nu}$) at the CERN SPS. J. Phys. Conf. Ser. **1526**, 012028 (2020). https://doi.org/10.1088/1742-6596/1526/1/012028
62. R. Chehab, R. Cizeron, C. Sylvia, V. Baier, K. Beloborodov, A. Bukin, S. Burdin, T. Dimova, A. Drozdetsky, V. Druzhinin, M. Dubrovin, V. Golubev, S. Serednyakov, V. Shary, V. Strakhovenko, X. Artru, M. Chevallier, D. Dauvergne, R. Kirsch, J.-C. Ph Lautesse, J. Poizat, A. Remillieux, P. Jejcic, J. Keppler, L. Major, G. Gatignon, V. Bochek, N. Kulibaba, A. Maslov, A. Bogdanov, I. Vnukov. Potylitsin, Experimental study of a crystal positron source. Phys. Lett. B **525**(1–2), 41 (2002). https://doi.org/10.1016/S0370-2693(01)01395-8
63. X. Artru, R. Chehab, M. Chevallier, V.M. Strakhovenko, A. Variola, A. Vivoli, Polarized and unpolarized positron sources for electron–positron colliders. Nucl. Instrum. Methods Phys. Res. B **266**, 3868 (2008). https://doi.org/10.1016/j.nimb.2008.02.086
64. X. Cheng-Hai, R. Chehab, P. Sievers, X. Artru, M. Chevallier, O. Dadoun, G.-X. Pei, V.M. Strakhovenko, A. Variola, A positron source using an axially oriented crystal associated to a granular amorphous converter. Chin. Phys. C **36**(9), 871 (2012). https://doi.org/10.1088/1674-1137/36/9/014
65. I. Chaikovska, R. Chehab, A. Faus-Golfe, Y. Han, S. Ogur, K. Oide, Y. Papaphilippou, L. Rinolfi, P. Sievers, F. Zimmermann, Y. Enomoto, K. Furukawa, T. Kamitani, F. Miyahara, M. Satoh, Y. Seimiya, T. Suwada, A. Apyan, P. Martyshkin, Positron source for FCC-ee, in *Proceedings of the 10th International Particle Accelerator Conference (IPAC'19)*, Melbourne, Australia, 19–24 May 2019, paper MOPMP003 (2019), p. 424. https://ipac2019.vrws.de/papers/mopmp003.pdf. Accessed 12 Nov 2021
66. V.G. Baryshevskii, I.Ya. Dubovskaya, Complex and anomalous Doppler effect for channelized positrons (electrons). Soviet Physics Doklady **21**, 741 (1976)
67. M.A. Kumakhov, On the theory of electromagnetic radiation of charged particles in a crystal. Phys. Lett. A **57**(1), 17 (1976). https://doi.org/10.1016/0375-9601(76)90438-2
68. A. Wu Chao, K.H. Mess, M. Tigner, F. Zimmermann, *Handbook of Accelerator Physics and Engineering* (World Scientific, Singapore, 2013). https://doi.org/10.1142/8543
69. A.I. Sytov, V.V. Tikhomirov, L. Bandiera, Simulation code for modeling of coherent effects of radiation generation in oriented crystals. Phys. Rev. Accel. Beams **22**, 064601 (2019). https://doi.org/10.1103/PhysRevAccelBeams.22.064601
70. A. Sytov, V. Tikhomirov, CRYSTAL simulation code and modeling of coherent effects in a bent crystal at the LHC. Nucl. Instrum. Methods Phys. Res. B **355**, 383 (2015). https://doi.org/10.1016/j.nimb.2015.02.042
71. L. Bandiera, E. Bagli, V. Guidi, V.V. Tikhomirov, RADCHARM++: a C++ routine to compute the electromagnetic radiation generated by relativistic charged particles in crystals and complex structures. Nucl. Instrum. Methods Phys. Res. B **355**, 44 (2015). https://doi.org/10.1016/j.nimb.2015.03.031
72. G.I. Marchuk, *Methods of Numerical Mathematics* (Springer, Berlin, 1975)
73. A.A. Samarskii, A.V. Gulin, *Numerical Methods* (Nauka, Moscow, 1989)
74. A. Mazzolari, A. Sytov, L. Bandiera, G. Germogli, M. Romagnoni, E. Bagli, V. Guidi, V.V. Tikhomirov, D. De Salvador, S. Carturan, C. Durigello, G. Maggioni, M. Campostrini, A. Berra, V. Mascagna, M. Prest, E. Vallazza, W. Lauth, P. Klag, M. Tamisari, Broad angular anisotropy of multiple scattering in a Si crystal. Eur. Phys. J. C **80**, 63 (2020). https://doi.org/10.1140/epjc/s10052-019-7586-6
75. V.V. Tikhomirov, A benchmark construction of positron crystal undulator (2015), pp. 1–27. arXiv:1502.06588v1
76. V.N. Baier, V.M. Katkov, V.M. Strakhovenko, *Electromagnetic Processes at High Energies in Oriented Single Crystals* (World Scientific, Singapore, 1998)
77. A.I. Sytov, V.V. Tikhomirov, A.S. Lobko, Crystal collimator systems for high energy frontier. Phys. Rev. Accel. Beams **20**, 071001 (2017). https://doi.org/10.1103/PhysRevAccelBeams.20.071001
78. V.V. Tikhomirov, A.I. Sytov, The miscut angle influence on the future LHC crystal based collimation system. Probl. Atom. Sci. Technol. **57**(N1), 88 (2012). http://dspace.nbuv.gov.ua/handle/123456789/107002. Accessed 12 Nov 2021
79. I.V. Kirillin, Optimal radius of crystal curvature for planar channeling of high-energy negatively charged particles in a bent crystal. Phys. Rev. Accel. Beams **20**, 104401 (2017). https://doi.org/10.1103/PhysRevAccelBeams.20.104401
80. I.V. Kyryllin, N.F. Shul'ga, Energy dependence of the efficiency of high-energy negatively charged particle beam deflection by planar channeling in a bent crystal. Eur. Phys. J. C **79**, 1015 (2019). https://doi.org/10.1140/epjc/s10052-019-7517-6
81. G. Celler, S. Cristoloveanu, Frontiers of silicon-on-insulator. J. Appl. Phys. **93**(9), 4955 (2003). https://doi.org/10.1063/1.1558223
82. J. Czochralski, Ein neues verfahren zur messung der kristallisations geschwindigheit der metalle. Z. Phys. Chem. **92**, 219 (1918). http://ci.nii.ac.jp/naid/10018467054/en/. Accessed 12 Nov 2021
83. Yu.M. Ivanov, A.A. Petrunin, V.V. Skorobogatov, Observation of the elastic quasi-mosaicity effect in bent silicon single crystals. JETP Lett. **81**, 99 (2005). https://doi.org/10.1134/1.1897998
84. R. Camattari, V. Guidi, V. Bellucci, A. Mazzolari, The 'quasi-mosaic' effect in crystals and its applications in modern physics. J. Appl. Cryst. **48**, 977 (2015). https://doi.org/10.1107/S1600576715009875
85. Ch. Wiebers, M. Holz, G. Kube, D. Nölle, G. Priebe, H.-Ch. Schröder, Scintillating screen monitors for transverse electron beam profile diagnostics at the European XFEL, in *Proceedings of the 2nd International Beam Instrumentation Conference (IBIC'13)*, Oxford, UK, Sep. 2013, paper WEPF03 (2013), p. 807. https://accelconf.web.cern.ch/IBIC2013/papers/wepf03.pdf. Accessed 12 Nov 2021
86. M. Werner, Re. Neumann, J. Lund-Nielsen, N. Wentowski, Sensitivity optimization of the standard beam current monitors for XFEL and FLASH II, in *Proceedings of the 10th European Workshop on Beam Diagnostics and Instrumentation for Particle Accelerators (DIPAC'11)*, Hamburg, Germany, May 2011, paper MOPD65 (2011), p. 197
87. M. Werner, T. Lensch, J. Lund-Nielsen, R. Neumann, D. Noelle, N. Wentowski, A toroid based bunch charge monitor system with machine protection features for FLASH and XFEL, in *Proceedings of the 3rd International Beam Instrumentation Conference (IBIC'14)*, Monterey, CA, USA, Sep. 2014, paper WEPF02 (2014), p. 521. https://epaper.kek.jp/IBIC2014/papers/wepf02.pdf. Accessed 12 Nov 2021
88. D. Lipka, W. Kleen, J. Lund-Nielsen, D. Nölle, S. Vilcins, V. Vogel, Dark current monitor for the European XFEL, in *Proceedings of the 10th European Workshop on Beam Diagnostics and Instrumentation for Particle Accelerators (DIPAC'11)*, Hamburg, Germany, May 2011, paper WEOC03 (2011), p. 572. https://accelconf.web.cern.ch/DIPAC2011/papers/weoc03.pdf. Accessed 12 Nov 2021
89. D. Lipka, J. Lund-Nielsen, M. Seebach, Resonator for charge measurement at REGAE, in *Proceedings of the 2nd International Beam Instrumentation Conference (IBIC'13)*, Oxford, UK, Sep. 2013, paper WEPF25 (2013), p. 872
90. M.G. Minty, F. Zimmermann, *Measurement and Control of Charged Particle Beams* (Springer, Berlin, 2003)